Fresenius J Anal Chem (2000) 366 : 712–726

REVIEW

R. Salzer · G. Steiner · H. H. Mantsch · J. Mansfield
E. N. Lewis

Infrared and Raman imaging of biological and biomimetic samples

Received: 4 October 1999 / Revised: 13 December 1999 / Accepted: 15 December 1999

Abstract Established methods for imaging of biological or biomimetic samples, such as fluorescence and optical microscopy, magnetic resonance imaging (MRI), X-ray tomography or positron emission tomography (PET) are currently complemented by infrared (both near-IR and mid-IR) as well as Raman spectroscopic imaging, whether it be on a microscopic or macroscopic scale. These vibrational spectroscopic techniques provide a wealth of information without *a priori* knowledge of either the spectral data or the composition of the sample. Infrared radiation does not harm the organism, no electric potential needs to be applied, and the measurements are not influenced by electromagnetic fields. In addition, no extrinsic labeling or staining, which may perturb the system under investigation, has to be added. The immense volume of information contained in spectroscopic images requires multivariate analysis methodologies in order to effectively mine the chemical and spatial information contained within the data as well as to analyze a time-series of images in order to reveal the origin of a chemical or biochemical process. The promise and limitations of this new analytical tool are surveyed in this review.

R. Salzer (✉) · G. Steiner
Technische Universität Dresden, Institut für Analytische Chemie, 01062 Dresden, Germany

H. H. Mantsch · J. Mansfield[1]
Institute for Biodiagnostics, National Research Council, 435 Ellice Avenue, Winnipeg, Manitoba, Canada R3B 1Y6

E. N. Lewis[2]
Laboratory of Chemical Physics, National Institute of Diabetes, Digestive and Kidney Diseases, National Institute of Health, Bethesda, Maryland 20892, USA

Present address:
[1] Hypermed Imaging Inc., 230 Second Avenue, Waltham, MA, 02451, USA
[2] Spectral Dimensions, Inc, 3403 Olandwood Court Suite 102, Olney, MD 20832, USA

Introduction

It is an old dream of scientists, engineers and physicians to be able to generate high-fidelity chemical images alongside conventional optical images. Chemical images such as these should be rapidly obtainable and should be of high spatial and energetic resolution. Within recent years, a new imaging technique has emerged which serves this goal: focal plane array detectors (FPA) coupled to near-IR, mid-IR or Raman spectrometers produce spatially-resolved spectral information in a short observation time. A wealth of information can be derived from the intrinsic characteristics of the vibrational images thus obtained. Most importantly, no sophisticated markers have to be added in order to determine the presence and distribution of the chemical constituents (Fig. 1) [1]. The contrast in vibrational images is solely derived from differences in the spectral and spatial heterogeneity of the biochemical components. Therefore, a single imaging data set contains an inherent multiplicity of contrast-producing mechanisms that arise from differences in the biochemical composition [2] (Fig. 2). This type of spectroscopic imaging is typically referred to as hyperspectral imaging because of the additional chemical or spectra dimensionality afforded over conventional optical imaging by the ability to image the sample at a number of different optical wavelengths or frequencies. Each spectral channel or image slice can be considered as another chemical probe or dimension to the data. So far, the lack of appropriate *in-situ* imaging techniques imposed certain limits to investigations [3]. Existing microscopic raster-scanning techniques cannot repeatedly be applied because of the extremely high time demand of 15 to 20 h per chemical image. Over such extended measuring times, on-going processes within a biological sample may have been disturbed or a synthesized sample may have undergone changes.

Most of the array detectors used nowadays for mid-IR chemical imaging have been developed for military applications. They became available for civil application in the early nineties [4, 5]. The first commercial mid-IR imaging

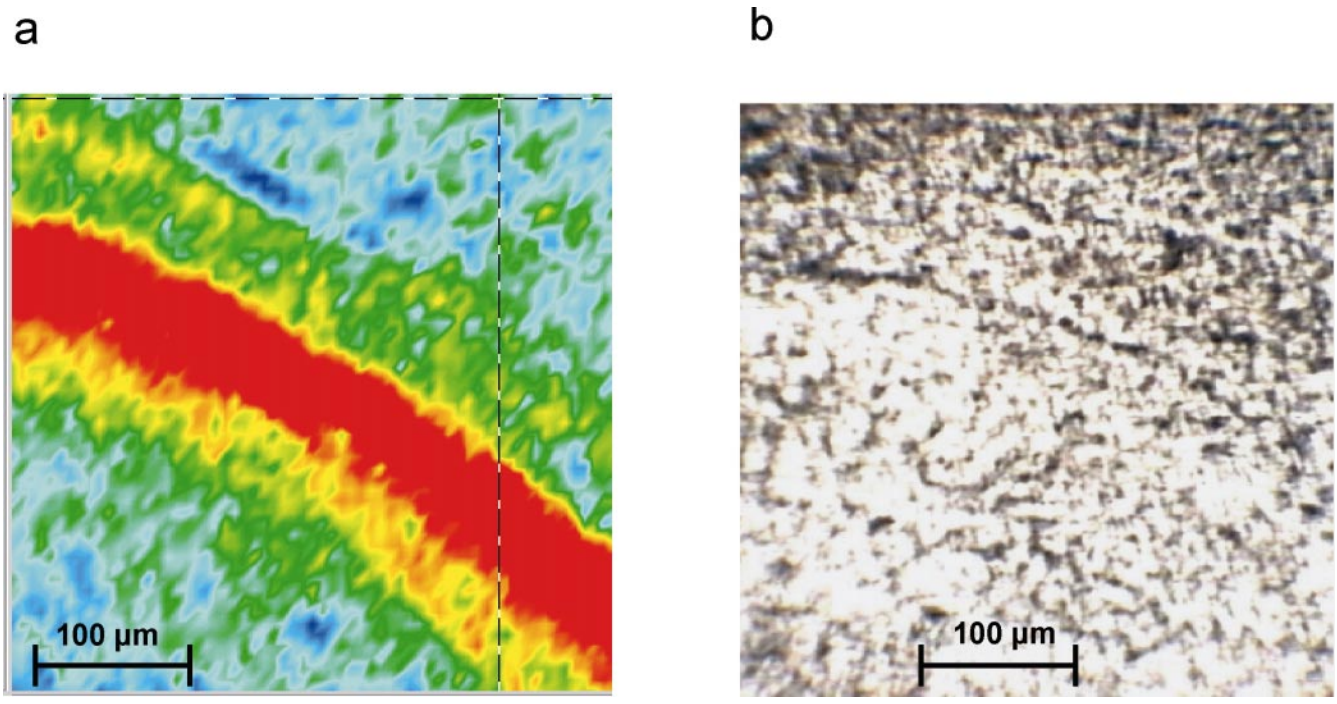

Fig. 1 a, b Mid-IR and VIS transmission images of a brain tissue section of a rat, sample size approx. $400 \times 400\ \mu m^2$. The tissue section was transferred onto a CaF_2 window and air dried. The image area per pixel of the 64×64 MCT detector array meets the size of a single biological cell. (**a**) Mid-IR image of the protein/lipid ratio determined from the band intensities at 3293 cm^{-1} (N-H str) and 2926 cm^{-1} (C-H str); red color indicates high values, blue color low values. (**b**) Microscopic image in the visible range; due to the alignment of the CCD camera with respect to the IR camera the VIS image is rotated counter-clockwise by approx. 10°

spectrometer appeared on the market soon afterwards. Presently, the main application fields for imaging spectrometers in civil research are biomedical diagnosis and polymer research. In polymer research, IR imaging has been applied to analyze the static and dynamic behavior of multi-component systems [6]. These include diffusion, phase separation, and identification of the different components [7]. IR imaging has allowed dynamic processes with a half-life of three minutes to be followed, e.g. polymer dissolution. Raman imaging has revealed the spatial distribution of crystallinity of syndiotactic polystyrene after all other instrumental methods failed [8]. Moreover, the chemical heterogeneity in emulsion systems, an important feature in understanding the microstructure of commercial products, could be described by Raman imaging as well [9]. The course of solid-phase combinatorial syntheses has been monitored and multiple products have successfully been characterized by near-IR imaging [10].

Bioanalytical imaging

One of the best known examples to demonstrate the promise of vibrational spectroscopy in bioanalytical applications is in the diagnosis of breast cancer [11], the most common malignant tumor among women. Breast cancer causes approximately 500.000 deaths each year world-wide. The conventional method for diagnosing and evaluating the prognosis is histopathological examination of biopsy samples. Even with the utilization of a clearly defined classification standard, pathologists do not always arrive at the same conclusion [12]. The search for more quantifiable methods, which can maintain existing visualization protocols while simultaneously adding a quantitative analytical aspect, has significant appeal. Vibrational spectroscopy has already shown its ability to meet the demands for more quantifiable results with virtually any kind of sample [13]. Its greatest promise consists in its inherent ability to detect chemical changes in biosamples even before they become morphologically apparent.

Unlike previous step-and-collect or mapping experiments, the new technique using FPAs is a true imaging technique, acquiring both spatial and spectral information simultaneously [14]. State-of-the-art commercial instruments are able to provide thousands of spectra with near-diffraction-limited spatial resolution and medium spectral resolution in only a few minutes. The huge gain in measurement speed in imaging is based on the simultaneous detection of several thousand spectra by individual pixels across the detector array. Sample domains of unexpected properties are uncovered because the total area is always surveyed. The disadvantage of current FPA technology is a slight variation of physical parameters between individual detector pixels.

In comparison to imaging, the time-consuming mapping technique (Fig. 3) relies on one single detector. The advantages of the mapping technique are mainly based on the practically invariant physical parameters of this detector during the experiment. This advantage may result in lower detection limits and/or a reduced danger of spectral

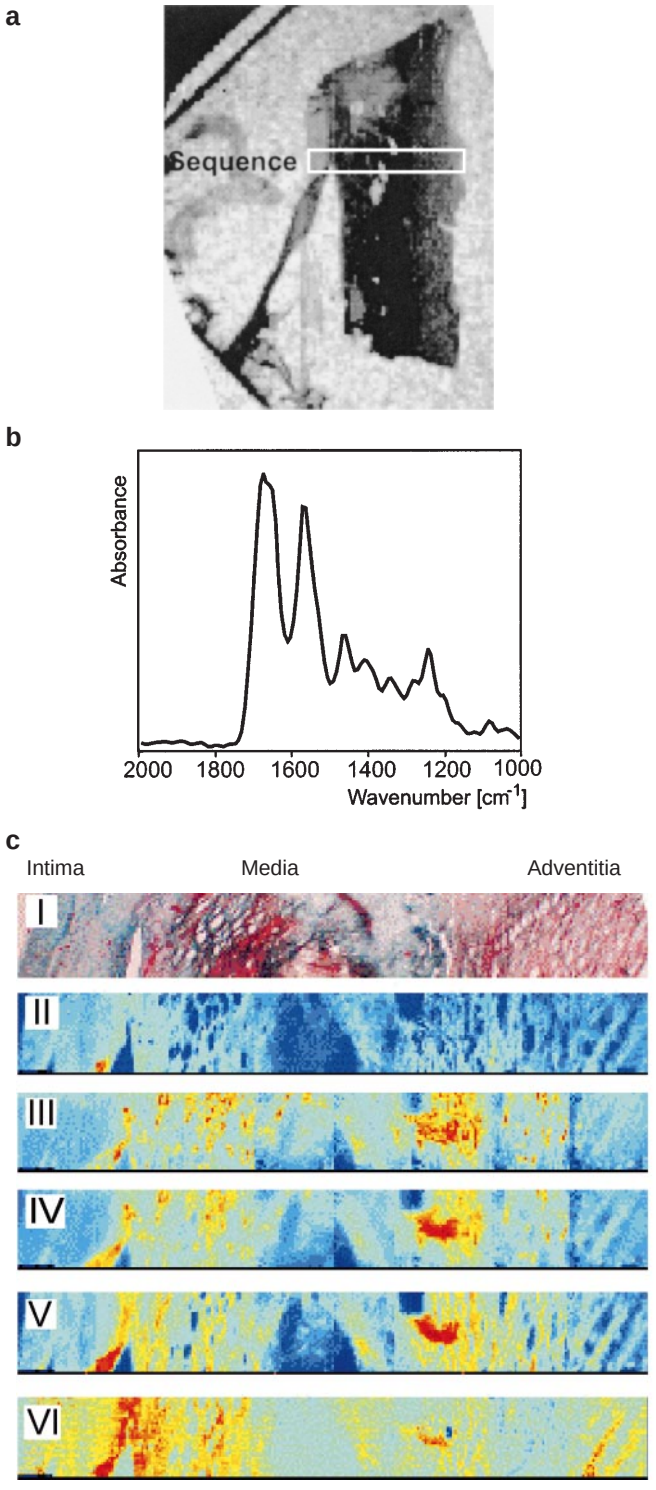

Fig. 2 a–c Mid-IR imaging of carotid plaques: (**a**) VIS micrograph of a transverse section across a human aorta wall. The interior part of the section (intima) is on the left side, the junction to muscular tissue (adventitia) on the right side. A continuous sequence of 64 × 64 images has been taken and pooled for evaluation. (**b**) Typical infrared spectrum of the intima area. (**c**) Histological (*I* - sudan stain) and FTIR spectral images of the transverse section across the human aorta (*II* - 1620 cm^{-1}; *III* - 1735 cm^{-1}; *IV* - 1170 cm^{-1}; *V* - 1655 cm^{-1}; *VI* - 1454 cm^{-1}). Red color indicates high values, blue color low values. New features are found particularly in *(V)* and *(VI)*, whereas *(III)* and *(IV)* resemble the conventionally stained image *(I)* more closely

artifacts. On the other hand, the lengthy measurement times in mapping experiments often require that a pre-selection of just a minimum number of positions across the sample area has to be made. The chances of finding domains with unexpected properties across the sample area are markedly reduced in this kind of supervised investigation. Obviously, mapping and imaging are to a large extent complementary.

Vibrational properties can be measured of any type of sample under any given physical conditions. This unique advantage together with the recent appearance of high-tech spectrometer components put high expectations on vibrational imaging and led to an increasing number of feature articles and accelerated papers appearing very recently [3, 15–18]. As with every emerging technique, the terminology has not yet been completely settled. The terms imaging (by taking all the spectra of the chosen sample area at once under an array detector without moving the sample, cf. Fig. 1) and mapping (by stepwise moving the sample under a single channel detector while taking a spectrum after each movement, cf. Fig. 3) are no longer disputed; however, the distinction between macro imaging and micro imaging is still ambiguous. For example, if a sample of 1 cm^2 size is imaged at a spatial resolution of less than 10 μm per pixel, its size is macro but its spatial resolution is micro. Clearly, the range of spatial scales that vibrational imaging can be applied to is enormous. There has a 13 order of magnitude size difference been reported for images collected on similar FPAs [17]. With respect to biomedical applications, the ambiguous terms macro imaging and micro imaging may be replaced by *in-situ* imaging and *ex-situ* imaging, because macroscopic measurements are usually performed under *in-situ* conditions, whereas microscopic measurements typically demand *ex-situ* conditions.

The recent technical development of focal-plane array detectors, tunable optical filters, as well as computer hardware and software enables us to exploit a variety of near-IR, mid-IR and Raman techniques for practical analytical applications [3]. The complementary mid-IR and Raman techniques both provide superior specificity due to their fingerprint capability. The advantage of NIR imaging is that its enhanced penetration depth makes analyses under *in-vivo* conditions possible [19]. In addition, near-IR data may contain contributions from electronic excitations together with the vibrational information [20]. This combination of electronic and vibrational information has been proven to provide specific insight into biochemical processes [21].

Thanks to the array detection, the time required for the data collection has been cut down by almost two orders of magnitude, presently to 1 to 15 min per data set. These experimental data are generated at such a fast rate (several megabytes per minute) that image processing often is becoming more demanding than the spectral measurement

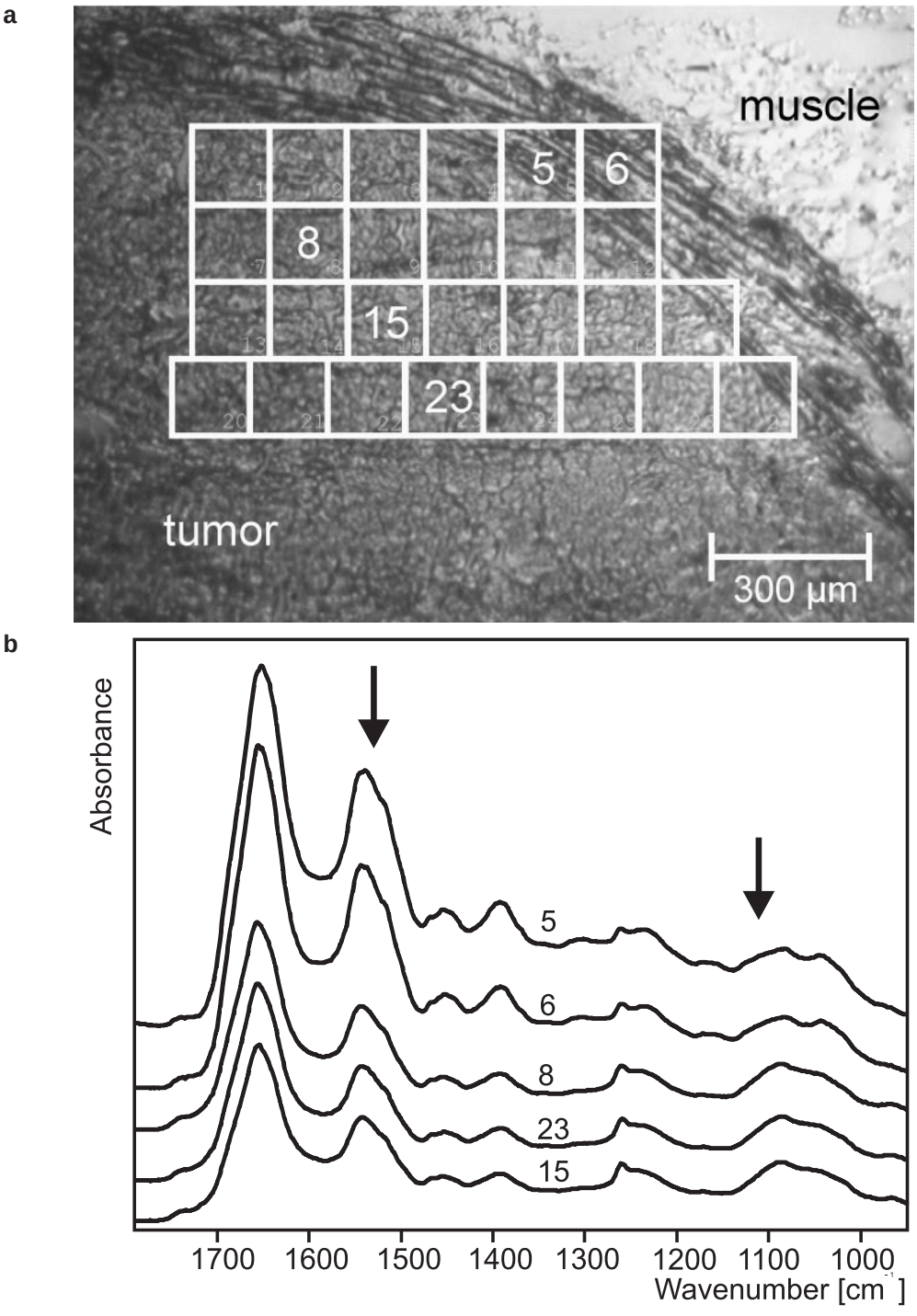

Fig. 3 a, b Mid-IR mapping of squamous cell carcinoma tissue. (**a**) VIS transmission image of a tumor section, the mapping positions are indicated. (**b**) Mid-IR microscope spectra of the selected sampling positions in (*a*). Arrows point to spectral regions showing distinct differences for different tumor areas. Sample spot sizes are 150 × 150 µm. The microscope is equipped with a computerized XY stage. The spectra are off-set for clarity

itself. The smallest FPA presently used in commercial instruments consists of 64 × 64 pixels. This FPA type already generates 4096 independent spectra per scan. Under such circumstances, the familiar problem of collecting a statistically required minimum number of independent data becomes more or less obsolete. The huge amount of spectral data now at hand leads to quite another problem: image construction algorithms are able to provide colorful images of reasonable appearance even from junk spectra if those algorithms are uncritically applied or used as black boxes. The necessity of carefully checking the experimental spectra behind the images has to be emphasized.

Conventional optical images are collected over the entire wavelength response range of a detector. Such images convey information about bulk properties of the sample such as topography, thickness or refractive index; however, they rarely contain specific chemical information. Those images will subsequently be referred to as bright-field images (Fig. 4 a). In contrast, an image sampled

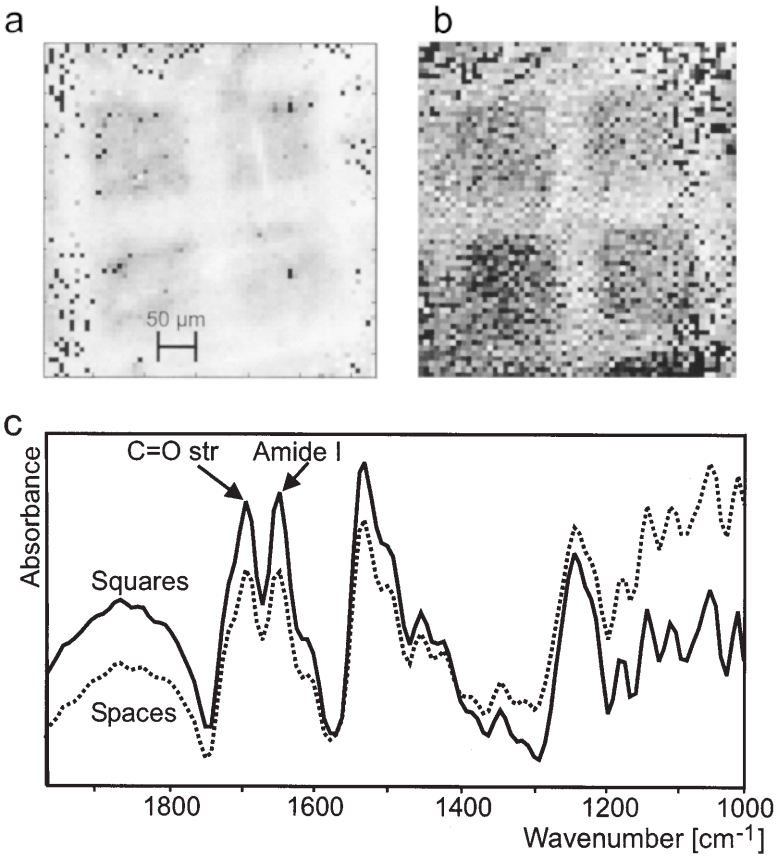

Fig. 4 a–c Microstructured biopolymer (poly-ε-benzoyl-carbonyl-L-lysine) grown on a self-assembled thiol monolayer. A thiol monolayer was formed on a CaF_2 substrate covered by a 50 nm gold layer. (**a**) Bright field transmission image (64 × 64 MCT detector array) of the mid-IR region 2000-900 cm^{-1} reveals topological information. The complete data set comprises 4096 IR spectra, total collection time is less than 10 min. Black spots in the boundary regions indicate bad pixels due to partial delamination of the detector array. (**b**) Spectral image computed from the same data by taking the ratio of the intensities of C = O stretching (1696 cm^{-1}) and amide I (1657 cm^{-1}) bands. Darker shades inside the squares indicate lower C = O/amide concentration ratios, brighter shades between the squares correspond to sites of increased C = O/amide concentration ratios. (**c**) Typical spectra (averages from 5 pixels) of the squares and the spaces between squares indicate the high sensitivity of the measurements

merely over a very limited wavelength range – usually one particular spectral band – is called a spectral image (Fig. 4b). Contrast in a chemical image as a function of absorption by a particular molecular functional group in the sample is often denoted a functional group image.

Biosystems are often far too complex to be fully explained in the traditional terms of functional group imaging. Ascertaining a biological response of a particular biofunctional system to an external stimulus may be more important than their investigation in terms of chemical composition. Ascertaining the biological or biochemical response is denoted functional imaging. The concepts behind functional imaging can be applied to a wide variety of problems, medical and non-medical, where the spatial and temporal response to an excitation is of interest.

Spectroscopic background

Spectra of biomolecules

Vibrational spectra of cells and tissues are dominated by bands due to proteins, since proteins are the most abundant species in cells (Fig. 5). Protein spectra in turn are dominated by the so-called amide I band between 1700–1600 cm^{-1} that is primarily associated with the stretching motion of the C = O unit within the amide group. This peak sensitively indicates changes in the neighborhood of the peptide linkage and provides excellent insight into the secondary structure of the protein [22]. The amide I band has already been used to image the microstructures in Fig. 4b. Weaker protein bands include the amide II band between 1580–1510 cm^{-1} (C-N stretching coupled to a CNH deformation motion), the amide III band between 1400-1200 cm^{-1} (coupled C-H/N-H deformation) and a number of side-chain vibrations. These weaker bands in the fingerprint region are often of higher diagnostic value [23] than broader bands such as those assigned to NH stretching vibrations (amide A around 3300 cm^{-1}, amide B around 3100 cm^{-1}).

Until recently, practically all vibrational studies on structural changes in proteins have used the mid-IR region and have concentrated on the conformation-sensitive amide I, amide II, and amide III modes. The well-established structure-spectra relationships of the mid-IR region [24] are now being correlated to features in less well understood spectral regions. The generalized 2-D correlation method developed by Noda [25] was successfully applied for monitoring structural changes of proteins in aqueous solution [26]. Near-IR wavelengths have been attributed by this method to secondary structural blocks of proteins [27]. A 2-D static correlation mode was developed in order to interpret structurally less clearly assigned bands, or possibly misassigned bands in other spectra [28]. Examples have been given for correlations of IR vs. Raman and Raman vs. circular dichroism [28].

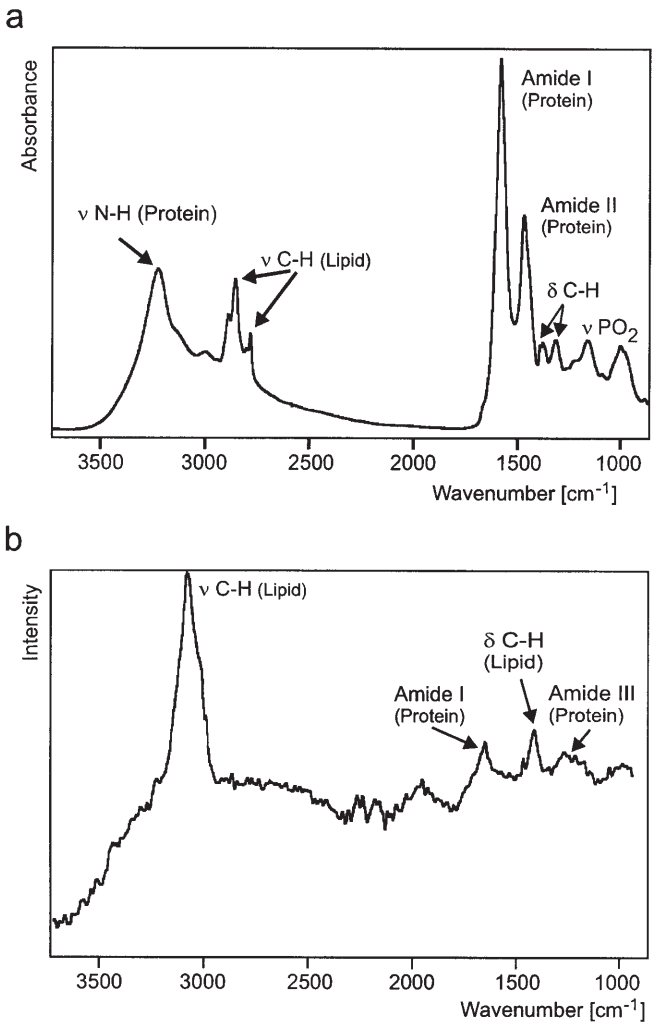

Fig. 5 a, b Representative microscopic spectra tissue sections: (**a**) IR spectrum; (**b**) Raman spectrum. The assignments of the major bands are indicated

Vibrational spectroscopic techniques

Vibrational techniques are easy-to-perform, non-destructive, are minimally invasive or even non-invasive [29]. IR spectroscopy has attracted great attention for biodiagnostic purposes [30]. One restriction in the mid-IR range is the requirement for tissue to be removed from subjects before analysis (*ex-vivo* investigation) [31]. However, this is not a serious restriction as biopsies are routinely taken for many conditions. Whether it is a mapping or imaging experiment, diffraction effects limit the spatial resolution in the mid-IR range (4000-400 cm^{-1} or 2.5-25 μm) to approx. 5-10 μm.

Most mid-IR imaging measurements are still performed in transmission mode. This is partly due to the fact that the microscopes that have been employed are modified single-point systems. As a result they are not optimized for imaging into an infrared focal-plane array detector and perform particularly poorly in reflectance where there is less opportunity to compensate for optical losses. More recently, an infrared microscope that was specifically designed for infrared imaging has appeared on the market. Recall that typical conventional measurements are assumed to be performed on optically homogeneous sample areas (diffuse reflection measurements are an exception in this regard), whereas images are only observed in the case of optically inhomogeneous samples. Nowadays, measurements of mid-IR external reflection

Fig. 6 a, b Cellular structure of untreated onionskin. (**a**) VIS bright-field image with the nucleus in the upper left part of the cell (15 × objective; 107 × 107 $μm^2$). (**b**) Spectral reflectance image (MCT detector array, 32 × 32 pixels shown) of the same area computed from the integrated intensity between 4550-4450 cm^{-1} in order to highlight the cellular contours. Red color indicates high values, blue color low values. Note the structural differences between (**a**) and (**b**) for the nucleus and the distribution of the cytoplasma at the cell border

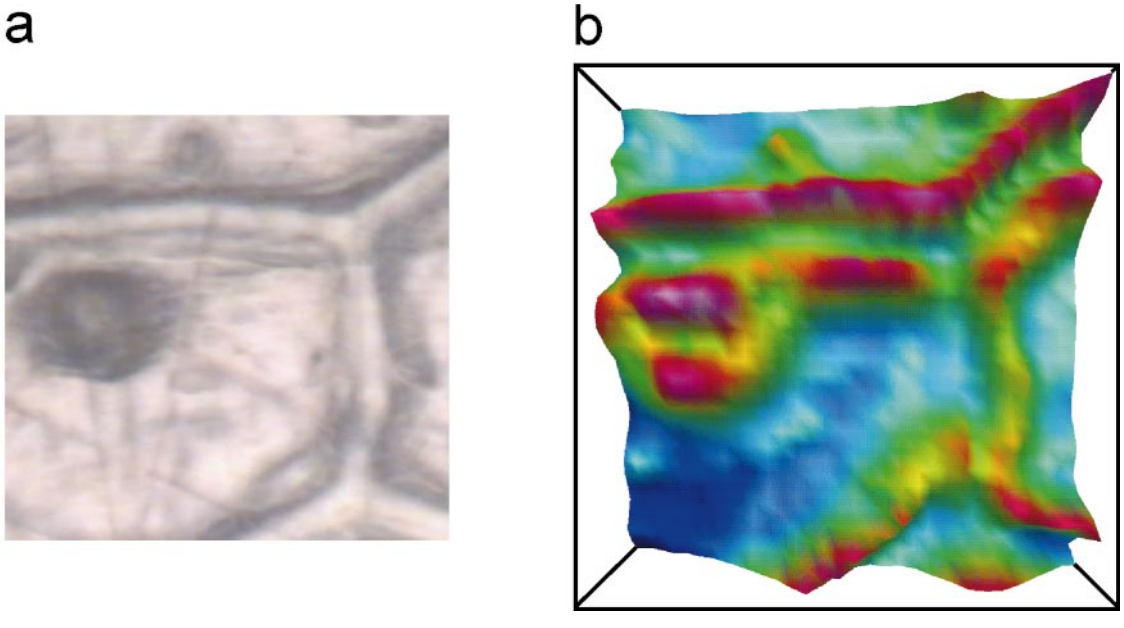

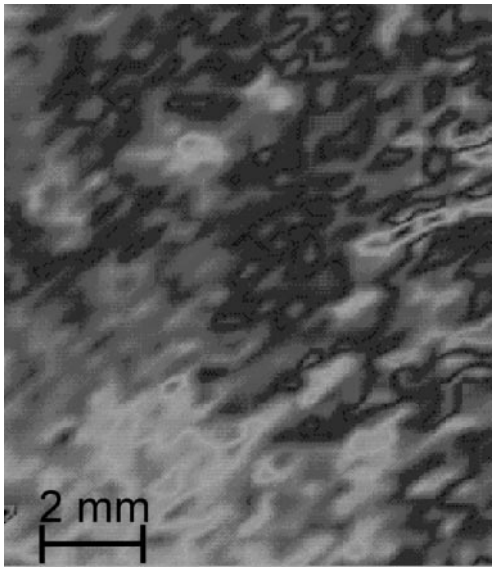

Fig. 7 IR ATR spectral image (64 × 64 MCT detector array) of a piece of ham. The intensity observed at 1535 cm^{-1} was used to construct the image. The sample was laid on the optical surface of a horizontal ATR crystal, no sample preparation was necessary

are easily accomplished (Fig. 6). Mid-IR imaging can even be done under ATR conditions (Fig. 7), which is an important step towards the fast *in-situ* analysis of biomaterial, e.g. the real-time analysis of tissue sections right in the operating theatre.

Early Raman measurements of biosamples were hindered by two problems [32]: (i) the often strong fluorescence within these samples and (ii) limitations in previous instrumentation, which necessitated high laser intensity and long exposure time in order to obtain spectra of good quality. Recent technical improvements helped remedy this situation, particularly upon excitation of the Raman spectra in the near-IR region [29], where fluorescence is widely reduced and the penetration depth of the radiation shows a maximum. In contrast to complementary IR spectroscopy, water is an ideal solvent in Raman spectroscopy, which makes *in-vivo* Raman measurements by fiber optic probes more feasible [33]. Typical acquisition times of less than 30 s have been reported for fiber-optic-based Raman *in-vivo* spectroscopy [34]. We want to make clear that the cited acquisition times hold for spectroscopy and not for imaging. In theory, the image quality in Raman microscopy should be superior to IR microscopy based on diffraction arguments, but the latter typically provides higher sensitivity and faster acquisition times [3]. *In-situ* Raman imaging of biological materials is typically not performed for this reason. The sensitivity and selectivity of Raman measurements may be improved (i) by utilization of surface enhancement (Surface Enhanced Raman Spectroscopy, SERS) [35] or (ii) by excitation in the UV range from 200 to 260 nm, where the Raman signals from aromatic amino acids as well as the purine and pyrimidine bases of nucleic acids and proteins are resonance enhanced (Resonance Raman Spectroscopy) [36]. However, based on existing technologies, *in-vivo* Raman imaging utilizing the SERS effect is unlikely to be practical.

The near-IR region is sometimes considered a compromise between the trade-offs that must be made in choosing between IR and Raman imaging. Near-IR spectral imaging just like IR spectral imaging should not be confused with IR thermography, where the thermal emission of the tissue is recorded. Near-IR spectral imaging relies on overtone and combination vibrational bands as well as low energy electronic transitions between 13 000 and 4000 cm^{-1} (770–2500 nm). Light of those wavelengths penetrates deeper into tissue than visible or mid-IR radiation. Spectral features are broad and weaker than the corresponding fundamental modes. Lower extinction coefficients, initially considered a drawback, allow thicker samples to be investigated, and they cause an extended linear range of the Lambert-Beer law. *In-vivo* monitoring by near-IR reflectance imaging has already been introduced into the clinic [21]. The near-IR reflectance of tissue is governed by the absorbance of the tissue as well as its bulk scattering properties. Powerful multivariate statistical methods permit the extraction of chemical and spatial information [19].

One lasting reservation concerns the separability among particular classes of organic compounds found in the near-IR range. Recently, this question was explored both qualitatively and quantitatively [37]. While there is more chemical specificity in the IR region 2500 to 500 cm^{-1} there is sufficient specificity throughout the near-IR region to allow organic compounds of one class to be identified and quantified in the midst of interference from the other classes. In conclusion, near-IR spectroscopy is not just a convenient tool for quantitative determinations of less complex mixtures. The combination of superior technical properties, larger penetration depth and particular information content currently makes near-IR among the first choices as an *in-vivo* imaging technique.

Instrumentation for vibrational imaging

In order to build a spectroscopic imaging system, one needs two major components: a camera with which to collect images, and some means of selecting the wavelengths at which images will be collected. For Fourier transform instruments, images are acquired as a function of mirror displacement of a Michelson interferometer, and the resulting interferogram-based spectroscopic imaging data cube is later Fourier transformed, giving the final spectroscopic data set. Fourier transform instruments have to be operated in the step-scan mode in order to collect a complete image at each particular mirror position [5]. For non-Fourier transform instruments, images are collected using some form of a bandpass filter to allow through to the camera only a narrow portion of the light to which the camera is sensitive. The simplest means of accomplishing this is to use a set of bandpass filters, often mounted in a wheel-like apparatus for ease of switching and to change

the filters with each image. This method, while useful, can be cumbersome.

Two other means of accomplishing this separation are acousto-optical tunable filters (AOTF) and liquid crystal tunable filters (LCTF) [38]. While AOTF technology can be utilized to create near-IR spectrometers, image-quality AOTF crystals are difficult to produce and suffer from image blurring along one axis of the image. For this reason, LCTF technology has been much easier to apply. The optics are simpler (straight through for LCTFs and at an angle for AOTFs), resulting in a much easier marriage between filter and camera lens.

Charge Couple Device (CCD) cameras are commonly employed today. They are sensitive from 400 to 1100 nm. In order to get reasonable quality spectra, near-IR spectroscopic imaging application require a CCD camera with at least a 12-bit analog-to-digital (A/D) converter (4096 grayscale levels), and sometimes as high as a 16-bit A/D (65 536 grayscale levels). This increase in dynamic range is gained at the cost of speed, with the lower dynamic range camera systems being much faster. Front-illuminated CCD array elements have a maximum quantum efficiency (QE) of approximately 40%, while the more efficient back-illuminated CCD array elements have a maximum QE of approximately 80%, as well as a shift in maximum sensitivity towards the near-IR. For this reason, back-illuminated CCD elements are preferable for near-IR spectroscopic imaging applications.

The longer wavelength near-IR spectral region can also be accessed using InGaAS, InSb or PtSi array cameras. The detection regions for arrays of these types are very similar to the wavelength sensitivity regions of their single-pixel element versions and extend partly into the mid-IR region. A comprehensive review of IR detector arrays has recently been published [17]. The currently dominant array type for the mid-IR is the HgCdTe (MCT) detector, as in the case of the single-pixel element version. The technical breakthrough occurred after the hybrid principle was introduced for the construction of the array, i.e. the photon detection and the signal readout were separated into two semiconductor layers. Intended for use in thermal imaging systems the two layers of the hybrid arrays start to disintegrate after a large number cool-thaw-cycles because of the thermal mismatch of the two layers. Average lifetimes of MCT arrays are between 1 and 2 years if not kept permanently at liquid nitrogen temperatures. The replacement costs for a 64×64 MCT arrray amount to approx. $5000, rising significantly with increasing pixel numbers. Other types of infrared array detectors such as InSb or uncooled cameras have significantly longer lifetimes.

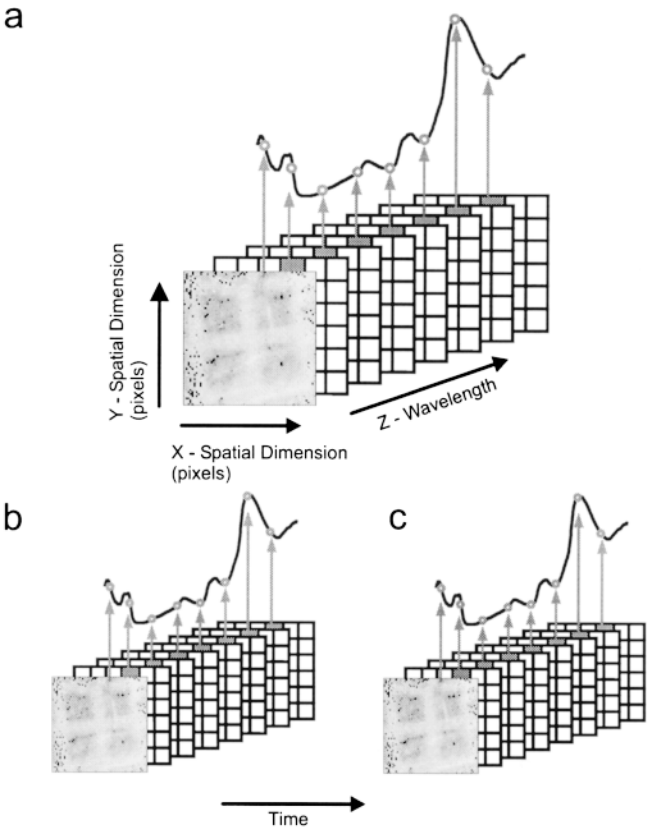

Fig. 8 a–c Spectroscopic imaging data cube. (**a**) Each slice of the data cube in the xy directions represents an spectral image taken by the detector array at a particular wavelength or at a particular mirror position in the case of a Fourier transform instrument. A spectrum is obtained from the series of consecutive pixels in the z direction. (**b**, **c**) Measurement series may be evaluated in a variety of ways depending upon instrumentation used (Fourier transform/non-Fourier transform) and parameters observed

Processing

Figure 8 a shows a representation of a spectroscopic imaging data cube. The resulting data set is a three-dimensional array of values with spatial distance in the x and y dimensions and wavelength or frequency along the z dimension. Slices of the array along the x, y directions and perpendicular to the z direction provide images at individual wavelengths, frequencies or mirror positions, depending on the data collection methodology, while rows of data extracted along the z direction provide individual spectra of interferograms from particular spatial locations. The two spectroscopic imaging data cubes in Fig. 8 b represent spectroscopic imaging data collected over time. The result of this is a four-dimensional data set which can be analyzed in a variety of ways.

Given the size of these multi-dimensional data sets which can sometimes be larger than 100 MB, it is not surprising that much work is being focused on developing processing methodologies to extract relevant information and reduce the size and complexity of the data down to a more manageable and information-rich set [39].

Image analysis

For some applications, viewing images simply taken at a single wavelength may suffice, or new images created

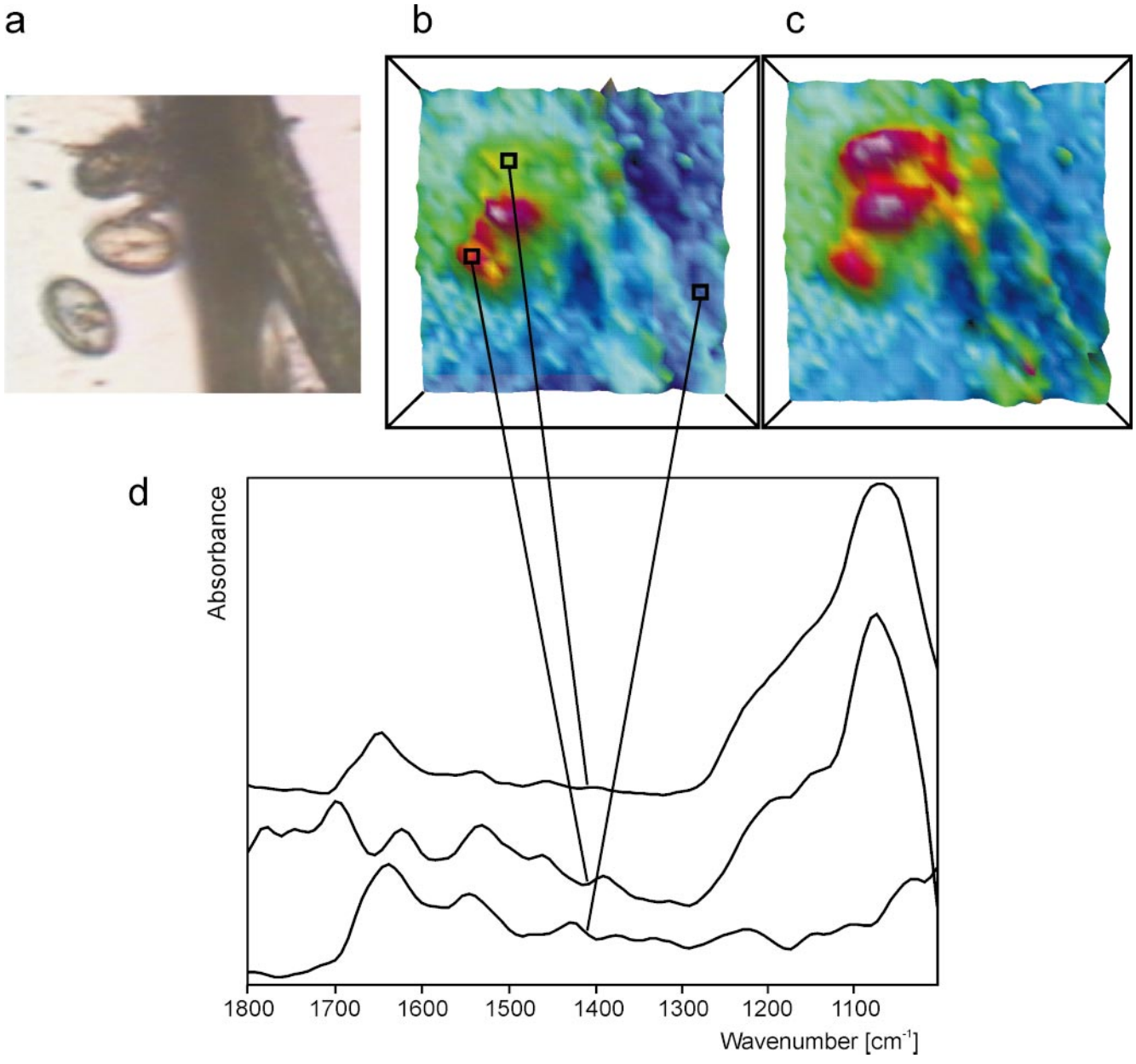

Fig. 9 a–d Algae from eutrophic waters, air dried on a CaF_2 window. (**a**) VIS bright-field image showing algae filaments and egg-shaped diatoms (15 × objective; 107 × 107 µm²). (**b**) Normalized spectral transmittance image (32 × 32 MCT detector array) of the same area computed as ratio of the integrated intensity in the range 1290-1010 cm^{-1} (silica, sugar, phosphates) divided by the intensity in the range 1700-1600 cm^{-1} (proteins). Red color indicates high values, blue color low values. Diatoms are easily located by their silica content emphasized after normalization. (**c**) This image was computed by subtraction instead of taking ratios. First a spectrum was extracted from the filament and subsequently subtracted from all spectra across the image (factor automatically adjusted for complete compensation of protein). Note the different image obtained by this procedure. (**d**) IR spectra for representative positions (silica/non-silica) in image (**b**)

from the difference or ratio between two individual wavelength images representing the maxima of two absorbances. Even though these simple approaches do not fully utilize the wealth of data contained in a spectroscopic image, they already provide rich structural insights. The single wavelength approach involves some risk of misinterpretation, because the depicted absorbance changes may be dominated or at least biased by variations in thickness across the sample layer. Such variations are common among biosamples, and the evaluation of band ratios is by far the safer choice (Fig. 9).

Analysis methodologies that use the entire spectral width of the data are more powerful than their discrete wavelength counterparts. Partitioning together those spectra that share common features into a small number of groups or classes is one means by which the large amounts of data can be reduced to a more meaningful and interpretable set. Two such classification methodologies are supervised classification, where the data are partitioned according to their similarity to pre-defined training

sets, and unsupervised classification, where the data are partitioned based solely on some measure of their variance without use of any *a priori* information. Each of these methodologies has its strengths and weaknesses, but the two are in many ways complementary. Unsupervised analyses, in conjunction with a variety of spectral normalization routines, are powerful exploratory tools, and, because they have a paradigm or model-free analysis methodology, they allow for the discovery of both novel and anticipated results. The usefulness of these methods in the analysis of a variety of near-IR spectroscopic imaging applications has been shown [40, 41]. Supervised classification methodologies, on the other hand, require some *a priori* knowledge of the data and the selection of pre-defined training sets against which to classify the data. This can be a limitation in data exploration but allows for a more precise classification within the boundaries determined by the choice of training sets [42, 43].

The spectra contained in a spectroscopic imaging data cube are in all ways identical to those acquired as a single spectrum. They may, therefore, be manipulated using all of the same tools used by spectroscopists for decades. This includes the taking of derivatives, the normalization of spectra, peak enhancement/deconvolution methods, offset corrections and more. Functional group mapping is the most frequently used approach to the analysis of spectroscopic maps. In functional group mapping, the integrated area, peak intensity, peak position or intensities of absorption bands arising from specific functional groups are plotted as a function of spatial position within the map. The functional group mapping approach is valuable, but it gives information only on a single peak. Taking the ratio of the intensity of two bands or the application of some multi-wavelength computational algorithm can produce a variety of functional group maps from a single image cube.

One other approach to display multi-wavelength components is composite imaging, which has been used extensivley to analyze visible and IR satellite geographical images [44, 45]. In composite imaging, the distribution of one feature/component of interest in an image is displayed in red, green or blue. The distributions of two other components are displayed with the remaining colors. Combining these individual color maps produces an RGB image that shows the distribution of all three features/components simultaneously. This technique allows the simultaneous display of up to 3 functional group maps in a manner that takes advantage of our mind's natural ability to detect subtle differences and patterns in color, shading and spatial positioning in 2-dimensional images. As applied to microscope maps of tissue samples, this technique can be quite useful, and has been given the term "digital staining" [46]. Digital staining remains subjective, however, as the spectral features corresponding to the component of interest in the tissue must still be chosen by the investigator. Subjectivity can be largely removed by the application of multivariate pattern recognition of classification techniques to spectroscopic maps [42, 47].

Unsupervised classification methodologies

Principal component (PC) analysis identifies directions (prinicpal components) along which the variance of the data is maximal. PC methods are a useful means of reducing an otherwise unmanageable number of individual wavelength images (sometimes more than 2000) to a smaller set of data, which sometimes contains useful information about the spatial variability of the spectra of the sample [48, 49]. However, there is no guarantee, theoretical or empirical, that identifying directions of maximal variance can or should differentiate distinct responses. If more than one response occur, there is no guarantee that each response will be assigned to one, and only one principal component.

Other unsupervised classification methods, such as hard k-means and fuzzy C-means clustering, can be used to group spectra based upon the degree of similarity between spectra. Unsupervised cluster analysis methods are generally excellent tools to use in the exploration of spectroscopic images because no previous knowledge of the sample is required and since they do not introduce bias into the analysis. As unsupervised analysis methodologies are model-free, unexpected as well as anticipated responses can be identified [50]. However, even in the exploratory phase of the analysis, the user should have a clear question about the sample in mind, and therefore analyze the data in a fashion appropriate for addressing this question.

Cluster analysis identifies regions of the sample that have a similar spectral response by clustering the spectra such that the differences in the intra-cluster spectral responses are minimized, while simultaneously maximizing the inter-cluster differences between spectral responses. In this implementation, the results of a cluster analysis include, for each cluster, the cluster centroid spectrum (*viz.*, the weighted mean spectrum for the cluster), and the corresponding cluster membership map (*viz.*, the spatial distribution of the cluster). Taken together, they answer two commonly posed questions about spectroscopic imaging: where did the different types of spectra occur (shown by the cluster membership maps, Fig. 10) and what were the spectral characteristics (depicted by the cluster centroids, Fig. 11).

Supervised classification methodologies

Once regions with specific components have been identified through exploratory unsupervised analyses, the location of those components can be more thoroughly investigated using a supervised classifier. Training set spectra required for the supervised classifier can be extracted from regions identified by the unsupervised analyses as containing a specific component, or they can be selected from the data set using previous knowledge of the composition of the sample. The supervised classifier can then refine the segmentation of the image by locating regions which have spectral profiles matching the training spectra (Fig. 12).

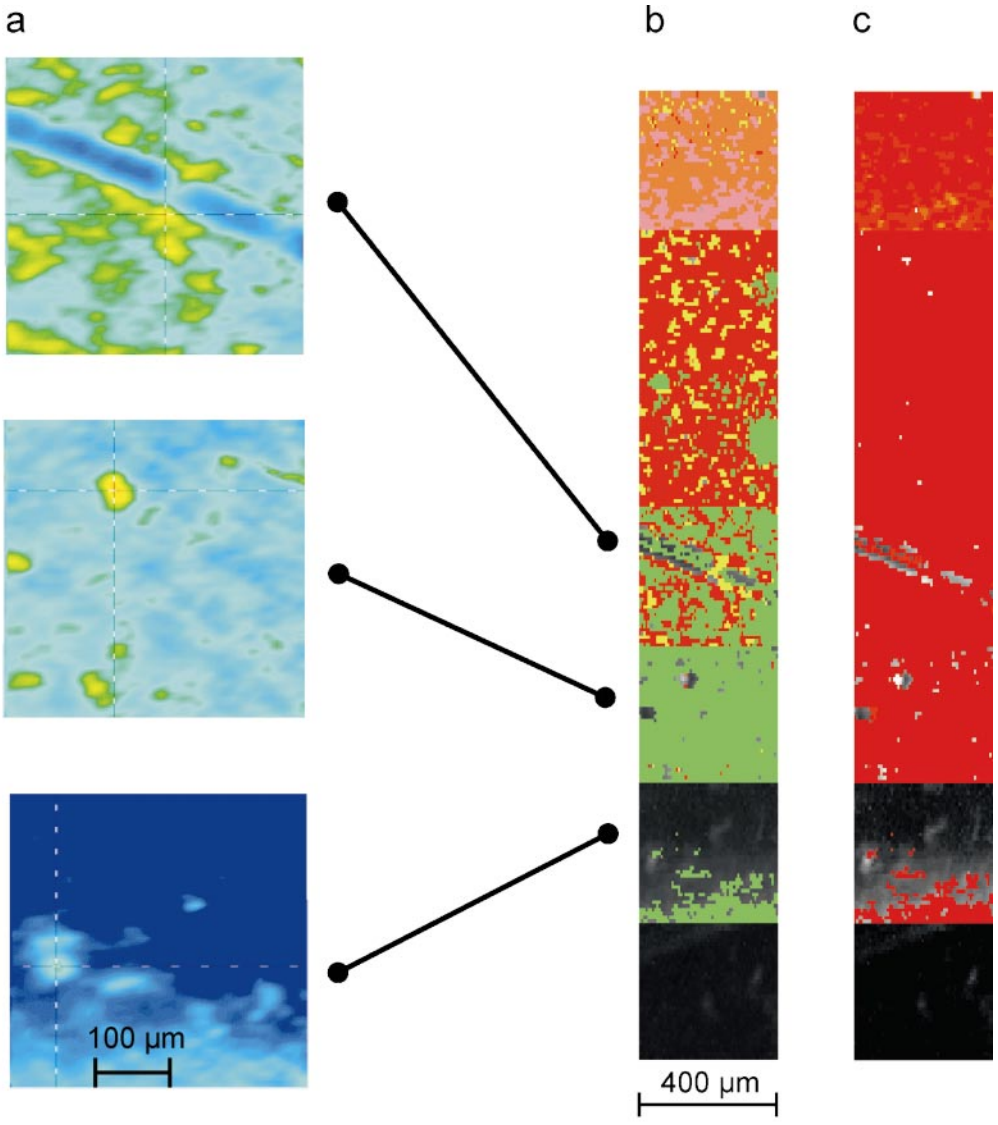

Fig. 10 a–c IR reflectance image of a biomineralized titanium surface. Thin layers of hydroxylapatite were synthesized under a variety of conditions. The uniformity of the non-crystalline layer (approx. 1 cm^2) was evaluated. (**a**) Individually evaluated IR reflectance images each covering an area of 400×400 μm^2 do not permit intercomparisons. Blue color indicates low values. (**b**) 7 representative IR images were combined into one contiguous file and subject to cluster analysis (C-means clustering). 5 distinct clusters were found (cf. Fig. 11 for the corresponding centroid spectra). Black areas indicate hydroxylapatite-free regions. (**c**) The distance between clusters is depicted by a correlation map. Larger distances are indicated by shades of orange. Faults in material are easily recognized by shades of gray [54]

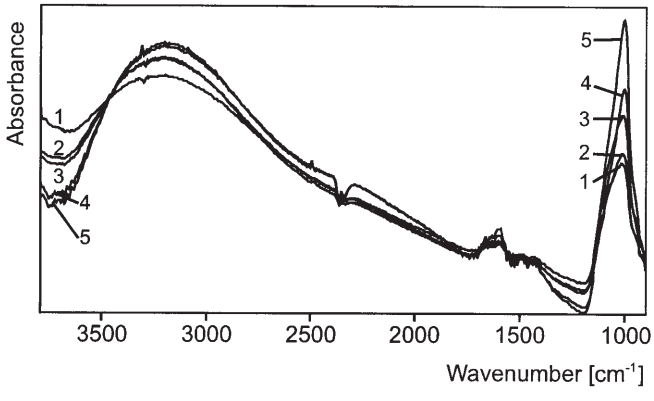

Fig. 11 Centroid spectra of the hydroxylapatite clusters shown in Fig. 10 b reveal the physical and chemical uniformity across the synthesized layer. Spectra *1–5* correspond to cluster colors red-orange-lilac-yellow-green. Physical uniformity is related to the particle size and is indicated by the stray light slope towards shorter wavelengths. The chemical uniformity is related to the phosphate/water ratio (band complexes at around 1000 cm^{-1} and 3200 cm^{-1})

Unsupervised analyses, combined with a supervised classifier, provide a means of locating the constituent components without *a priori* knowledge of number or nature of the components present in the sample. In addition, using the spectra selected for the training set as targets in library spectral search routines would also enable an automated identification of the components.

Supervised pattern recognition methods are potentially better suited to the development of clinically or industrially useful data analysis methods. Supervised pattern recognition techniques such as linear discriminant analysis [51] (LDA) or neural networks make use of the fact that the investigator often has a substantial amount of spectroscopic data available (either biochemical or clinical). For example, the investigator may know that spectra arise from well-defined sample components or tissue types. This information may then be used to train a LDA algorithm to recognize the particular combinations of variables (peak frequencies, bandwidths, relative intensities, etc.) in the spectra that are characteristic of these sample components or tissue types.

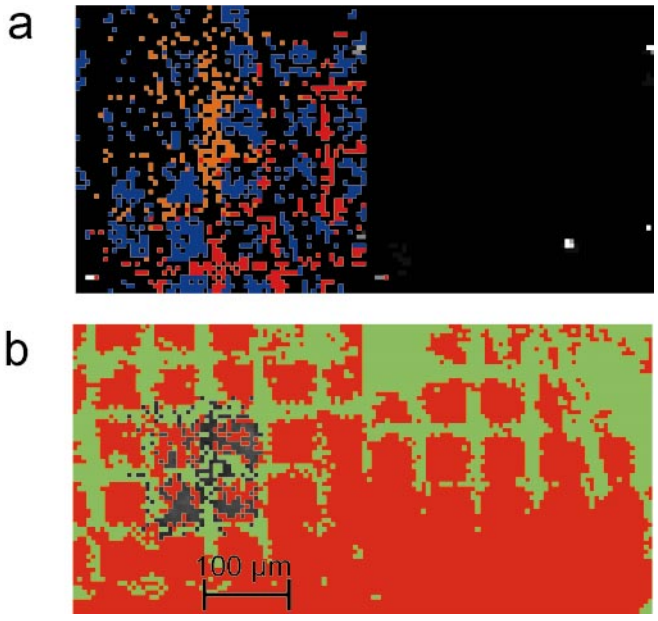

Fig. 12 Microstructured polystyrene grown on a self-assembled thiol monolayer. A thiol monolayer was formed on a CaF_2 substrate covered by a 50 nm gold layer. The stamped thiol squares are 50 µm across and 20 µm apart from each other. Two IR transmission images (64 × 64 MCT detector array) sampled at sites of different layer thickness are combined into one contiguous file. (**a**) Unsupervised classification (C-means clustering) recognizes microstructural patterns in a part of the image. (**b**) The central region of the identified clusters was used as input for a linear discriminant analysis (dark pixels). LDA reveals microstructures all over the sampled area, regardless of the difference in layer thickness

In-vivo applications

As an example of the image and spectral quality obtainable under *in-vivo* conditions a spectroscopic imaging data set acquired from the dorsal surface of the hand of a volunteer is used (Fig. 13). As a representation of the spectral variability of such a sample is difficult without some form of data processing, fuzzy C-means clustering was used to cluster together those spectra whose spectral shapes were most similar. In order to reduce the spectral variability due to offset from the unevenness of illumination across the curved surface of the hand, all of the optical density (OD) spectra in the data set were offset-corrected such that the OD value of the 980 nm water absorbance of each spectrum was set to 0.2 OD.

Figure 13 shows the results of clustering the spectra from the dorsal surface of the hand into five clusters.

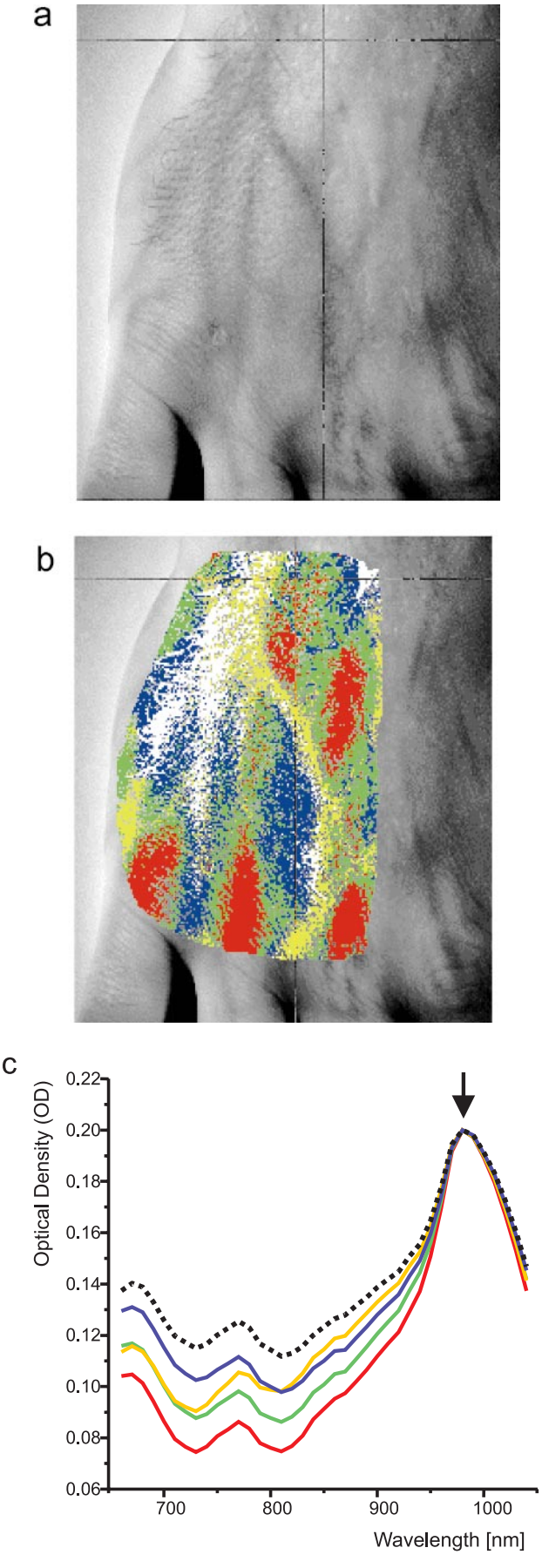

Fig. 13 a–c Results of an unsupervised classification (fuzzy C-means cluster analysis) of a spectroscopic image of the dorsal surface of a human hand. (**a**) A 760 nm reflectance image of the hand surface as a reference. (**b**) The 760 nm reflectance image of the dorsal surface of the hand with superimposed clustering results. (**c**) Shows the clusters centroid spectra, with the color of each spectrum corresponding to the color of the cluster result depicted in (**b**). The spectra were offset corrected at 980 nm (arrow) to reduce variability due to lighting

Figure 13a shows a 760 nm reflectance image of the hand as a reference. Figure 13b shows the spatial locations of the pixels comprising each of the clusters. Figure 13c shows the centroid, or average, spectrum from each of the five clusters. The color of the cluster shown in Fig. 13b matches the color of the centroid spectra shown in Fig. 13c (with the exception of the cluster shown in white, whose centroid spectrum is represented by a dashed line). The arrow shows the point at which the spectra were offset-corrected. The centroid spectra shown in Fig. 13c are good-quality spectra which match well with those collected using fiber optics, each exhibiting an obvious 760 nm deoxy-hemoglobin absorbance and a prominent 980 nm water absorbance. Closer examination reveals that the peak areas of both the deoxy-hemoglobin and water bands are approximately the same for each of the five clusters. The major difference between each of the centroid spectra lies in the depth of the curve between 650 and 950 nm as well as the slope of the spectra between 800 and 950 nm, both of which represent to some degree the scattering properties of the tissue and show the variability in scattering across the hand. This observation is critical for the assessment which of data analysis methodologies will be useful for such *in-vivo* data sets; those methods which assume homogeneity in the scattering properties of tissue will not be as useful as those which make no such assumption.

In addition to being used to analyze the spectral characteristics of a sample at a single time instance, spectroscopic imaging techniques can also be used to monitor changes in a sample over time. By collecting spectroscopic imaging data cubes (or relevant subsets of the entire cube) over time, a four-dimensional data set can be built up. A data set of this nature can be reduced to a more manageable size in a variety of ways (cf. Fig. 8b). The spectroscopic imaging data cubes from each time-point in the series can be individually analyzed for spatial variations in their spectra, individual wavelength images can be extracted from the data cube for each time-point and put together to form a time-series for a given wavelength, or some form of algorithm can be used on the spectra of each data cube to reduce it down to a single (or small number) of relevant images to form a time-series. Or, conversely, the entire set of spectra or the entire set of wavelength time-series can be pooled together for one large analysis. None of these, individually will allow for the full visualization of the information contained in the four-dimensional data set. However, taken together, they can allow the spectroscopist to understand the variations in the data more fully.

One example of this type of analysis is the assessment of cardiac oxygenation and perfusion. It is important during assessment of heart perfusion and ischemic damage models to be able to determine the regional oxygenation status of the cardiac tissue. To assess the usefulness of near-IR spectroscopic imaging in this arena, a crystalloid-perfused (i.e., not blood-perfused) arrested porcine heart model was used, with three different perfusion states being utilized [52]. Figure 14 shows fuzzy C-means clustering results from the data sets acquired from hearts with

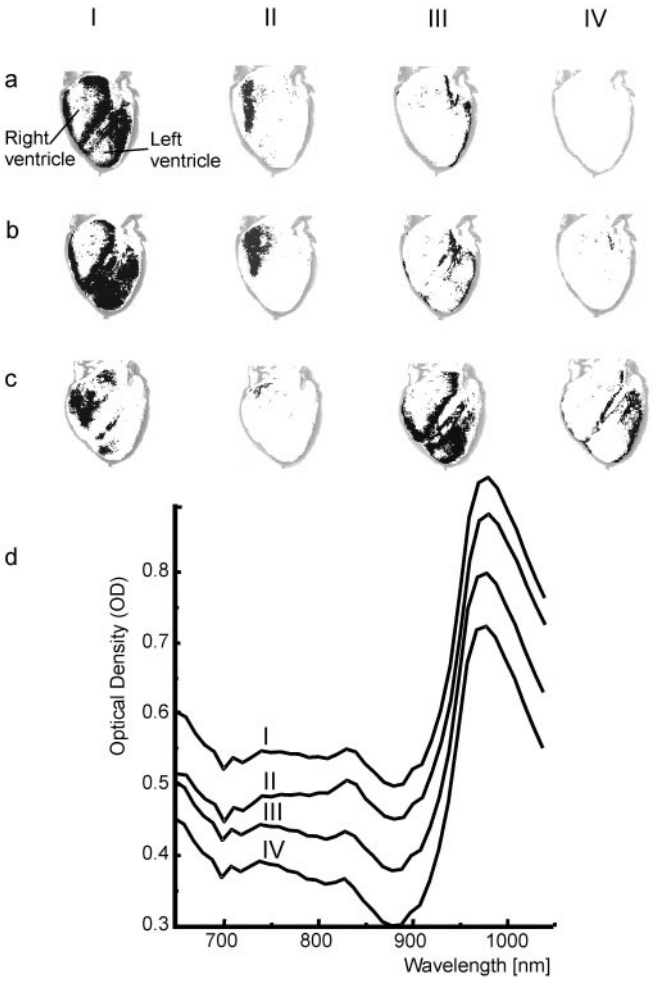

Fig. 14a–d Results of an unsupervised classification (fuzzy C-means clustering) of the pooled spectra from a near-IR spectroscopic image taken of a porcine heart undergoing three different perfusion states: normal perfusion, LAD artery occluded regional ischemia, and no-flow global ischemia. As the spectra were pooled prior to clustering, the clusters depicted in column I of (**a**)–(**c**), for example, all belong to the same biochemical situation represented by spectrum I in (**d**). (**a**) Clustering results superimposed on a 760 nm reflectance contour of the heart during normal perfusion. (**b**) depicts the clustering results superimposed on the left anterior descending (LAD) artery regional ischemia model, wherein the left ventricle has had its perfusion compromised. (**c**) Shows the clustering results superimposed on an image of the heart during complete ischemia (no flow). (**d**) Shows the cluster centroid spectra from each of the four clusters. The number of each spectrum corresponds to the number of the cluster depicted in (**a**), (**b**), and (**c**)

the three perfusion states. Figure 14d shows the centroid spectra from clustering analysis of the pooled set of spectra from all three data sets. As expected, the spectra match those acquired using fiber optic spectrometers [53]. The 760 nm deoxy-myoglobin band (as there is no hemoglobin in the crystalloid perfusate) is clearly larger in centroid spectra III and IV, which dominate the surface of the heart in Fig. 14c, in which there is no perfusion of the system, while those regions of clusters I and II, which dominate the surface of the heart in both perfused states (Figs. 14a and 14b), have less deoxy-myoglobin. What is also

noticeable is that while the oxygenation of the left ventricle is reduced on occlusion of the left anterior descending (LAD) artery, as is expected, the oxygenation of the right ventricle increased. This is due to the fact that the total perfusion flow was not altered during LAD artery occlusion, causing an overall increase in the perfusion rate to the right ventricle and resulting in an increase in myoglobin oxygenation.

Experimental

Near-IR spectroscopic images were collected using a Princeton Instruments charge coupled device (CCD) camera consisting of a 512 × 512 back-illuminated SiTe CCD element and a 16-bit ST-138 A/D converter (Princeton Instruments, Trenton, NJ). The images were collected as 256 × 256 arrays, binning the CCD in 2 × 2 squares. Wavelength selection was provided by a liquid crystal tunable filter (LCTF) unit from Cambridge Research Instruments (Cambridge, MA), which was used to scan through from 640 to 1040 nm at 10 nm intervals. Raw reflectance images were converted to an optical density scale by ratioing the reflectance images against images of a Kodak "Gray Card" white surface (Eastman Kodak, Rochester, NY) taken at the same wavelengths and illuminated identically to the images of the subjects [41]. This conversion to an optical density scale allowed the spectra in each data cube to be input into standard spectroscopic algorithms, as well, and simultaneously giving the images a flat-field correction to account for inhomogeneities in the lighting and any clipping of the image by the LCTF housing.

Mid-IR spectroscopic images shown in this paper were collected on different Bio-Rad Stingray instruments, on a Bruker Equinox 55/S equipped with an IRscope II microscope, as well as on a prototype of the InSight IR from SpectralDimensions (Olney/MD). MCT detector arrays operating at liquid nitrogen temperature were used in all instruments. Spectral resolution was typically set to either 8 or 16 cm^{-1}. Due to the chosen resolution it was not necessary to purge the optical path with dry gas. Single IR images were evaluated using software provided by the manufacturers as well as using the Matlab software package. Pooled IR images were evaluated using the 3D analysis package EvIdent (NRC, Institute for Biodiagnostics, Winnipeg).

Conclusions and outlook

Spatially resolved chemical information can be obtained for all kinds of molecules in their natural environment by IR and Raman imaging. The quality of the spectral data in the images compares reasonably well with the quality of spectra collected by traditional single-pixel detectors. Acquisition times for complete images amount to a few minutes, which leads to short total analysis times and permits near-process analyses. Measurements can be performed with the IR microscopes in either transmission or reflection modes. Presently, these advantages are mainly employed in polymer research and biomedical diagnosis.

Within a short time interval array detectors used in imaging spectrometers produce an enormous number of individual spectra and chemical images. Even the smallest detector array of 64 × 64 pixels provides 4096 complete spectra every few minutes. Such huge amounts of data can no longer be evaluated by traditional methods. New chemometric approaches need to be developed in order to locate not only expected, but more importantly, to detect unexpected events in the data stream. Common 2-dimensional computational procedures do fully interpret the data and for effective analysis we have to resort to multivariate methods. Among the existing multi-dimensional evaluation procedures, clustering analysis has proved to be extremely useful for the investigation of spectroscopic imaging data. It is robust, rapid, and non-subjective; and, as *a priori* knowledge of the spectral responses of the sample is not involved in the analysis, it allows for the discovery of both novel and anticipated features in the data. Cluster analysis, especially when combined with various spectral normalization routines, therefore makes an excellent exploratory tool. Supervised classification techniques, such as LDA, provide a much clearer picture of both the spectral and spatial properties of the sample. However, supervised methods required *a priori* knowledge of the spectral and spatial properties of the sample. These can be obtained either by prior knowledge of the chemical composition of the sample or by first performing a series of exploratory clustering analyses.

Current infrared and Raman imaging instruments are reliable and ready for routine applications, even though they represent a new generation of technology. On-going efforts, to open up more application areas by developing novel accessories, and by elaborating data evaluation strategies for spectral images will further improve the range of uses of spectral imaging. Combinatorial analysis as a complement to combinatorial synthesis will certainly be one of the areas with high application potential. Simultaneous processes in complex systems will soon be investigated under *in-situ* conditions, e.g. reactions inside nanostructured materials or within biological samples. The present bottleneck in spectral imaging, treatment of the vast amount of data, will be overcome by innovative strategies for evaluation of spectral information. Tens or even hundreds of thousands of spectra obtained day after day cannot anymore be treated in the approved classical manner. This development will likely proceed in a manner similar to that witnessed for the evaluation of near-IR spectral data which are typically treated in a statistical manner rather than by molecular-physical considerations.

Acknowledgements RS thanks the Dresden University of Technology for the permission for sabbatical leave. Most of the experiments shown were performed during this sabbatical. Hospitality and support at the National Institute of Health, Bethesda/MD (Dr. I. W. Levin), Rutgers University, Newark/NJ (Prof. Dr. R. Mendelsohn), Hospital of Special Surgery, New York City/NY (Dr. E. Paschalis), NRC Institute for Biodiagnostics, Winnipeg/Manitoba (Dr. R. Somorjai), are gratefully acknowledged. Thanks for sample preparation are expressed to Dipl.-Chem. V. Neumeister (TU Dresden), Dr. H.-G. Braun and Dipl.-Chem. Th. Kratzmüller (Institute for Polymer Research Dresden), Dr. M. T. Pham (Research Center Rossendorf). Financial support by the German Research Council, the Priority Program 287 of the German Research Council and the Fund of the Chemical Industry is gratefully acknowledged. Some of the results shown would not have been possible without support by Bio-Rad, Bruker Optik and SpectralDimensions.

References

1. Kidder LH, Kalasinsky VF, Luke JL, Levin IW, Lewis EN (1997) Nature Medicine 3:235
2. Lester DS, Kidder LH, Levin IW, Lewis EN (1998) Cellular Molec Biology 44:29
3. Lewis EN, Gorbach AM, Marcott C, Levin IW (1996) Appl Spectrosc 50:263
4. Lewis EN, Levin IW (1995) J Microsc Soc Amer 1:35
5. Lewis EN, Treado PJ, Reeder RC, Story GM, Dowrey AE, Marcott C (1995) Anal Chem 67:3377
6. Bhargava R, Wang SQ, Koenig JL (1998) Appl Spectrosc 52:323
7. Wall BG, Koenig JL (1998) Appl Spectrosc 52:1377
8. Zhang SL, Pezzuti JA, Morris MD, Appadwedula A, Hsiung CM, Leugers MA, Bank D (1998) Appl Spectrosc 52:1264
9. Andrew JJ, Browne MA, Clark IE, Hancewicz TM, Millichope AJ (1998) Appl Spectrosc 52:790
10. Fischer M, Tran CD (1999) Anal Chem 71:2255
11. Ci YX, Gao TY, Feng J, Guo ZQ (1999) Appl Spectrosc 53:312
12. Kidder LH, Haka AS, Faustino PJ, Lester DS, Levin IW, Lewis EN (1998) Proc SPIE 3257:178
13. Schrader B (1995) Infrared and Raman Spectroscopy, VCH Verlagsgesellschaft, Weinheim
14. Snively CM, Koening JL (1999) Appl Spectrosc 53:170
15. Treado PJ, Levin IW, Lewis EN (1992) Appl Spectrosc 46:1211
16. Lewis EN, Levin IW (1995) Appl Spectrosc 49:672
17. Colarusso P, Kidder LH, Levin IW, Fraser JC, Arens JF, Lewis EN (1998) Appl Spectrosc 52:106A
18. Diem M, Boydston-White S, Chiriboga L (1999) Appl Spectrosc 53:148A
19. Mansfield JR, Sowa MG, Mantsch HH (1999) Proc SPIE 3597:270
20. Sowa MG, Payette JR, Stranc MF, Abdulrauf B, Hewko MD, Mansfield JR, Mantsch HH (1998) Proc SPIE 3257:199
21. Payette JR, Sowa MG, Germscheid SL, Stranc MF, Abdulrauf B, Mantsch HH (1999) Amer Clinical Laboratory 18:4
22. Jackson M, Mantsch HH (1995) Crit Rev Biochem Mol Biol 30:95
23. Naumann D (1998) Proc SPIE 3257:235
24. Surewicz WK, Mantsch HH, Chapman D (1993) Biochemistry 32:389
25. Noda I (1993) Appl Spectrosc 47:1336
26. Schultz CP, Fabian H, Mantsch HH (1998) Biospectroscopy 4:19
27. Robert P, Devaux MF, Mouhous N, Dufour E (1999) Appl Spectrosc 53:226
28. Kubelka J, Pancoska P, Keiderling TA (1999) Appl Spectrosc 53:666
29. Schrader B, Dippel B, Fendel S, Freis R, Keller S, Löchte T, Riedl M, Tatsch E, Hildebrandt P (1998) Proc SPIE 3257:66
30. Shaw RA, Mantsch HH (1999) J Molec Spectrosc 480–481:1
31. Jackson M, Mantsch HH (2000) Encyclopedia of Analytical Chemistry, John Wiley (in press)
32. Mahadevan-Jansen A, Richards-Kortum R (1996) J Biomed Optics 1:31
33. Fendel S, Schrader B (1998) Fresenius J Anal Chem 360:609
34. Shim MG, Wilson BC, Marple E, Wach M (1999) Appl Spectrosc 53:619
35. Weldon MK, Morris MD, Harris AB, Stoll JK (1998) J Lipid Res 39:1896
36. Yazdi Y, Ramanujam N, Lotan R, Mitchell MF, Hittelman W, Richards-Kortum R (1999) Appl Spectrosc 53:82
37. Stallard BR (1997) Appl Spectrosc 51:625
38. Chrien TG, Chovit C, Miller PJ (1993) Proc SPIE 1937:256
39. Treado PJ, Morris MD (1994) Appl Spectrosc Reviews 29:1
40. Jackson M, Ramjiawan B, Hewko M, Mantsch HH (1998) Cell Mol Biol 44:89
41. Mansfield JR, Sowa MG, Scarth GB, Somorjai RL, Mantsch HH (1997) Anal Chem 69:3370
42. Mansfield JR, Sowa MG, Mazjels C, Collins C, Cloutis E, Mantsch HH (1999) Vibrational Spectrosc 19:33
43. Mansfield JR, McIntosh LM, Crowson AN, Mantsch HH, Jackson M (1999) Appl Spectrosc 53:1323
44. Cloutis EA (1996) Internat Remote Sensing 17:2215
45. Mumby PJ, Green EP, Clark CD, Edwards AJ (1998) Coral Reefs 17:59
46. McIntosh LM, Mansfield JR, Crowson AN, Mantsch HH, Jackson M (1999) Biospectrosc 5:265
47. Haaland DA, Jones HDT, Thomas EV (1997) Appl Spectrosc 51:340
48. Kawata S, Saskai K, Minami S (1987) J Optical Soc Amer A 4:2101
49. Mansfield JR, Sowa MG, Scarth GB, Somorjai RL, Mantsch HH (1997) Comp Med Imag Graph 21:299
50. Baumgartner R, Scarth G, Teichtmeister C, Somorjai RL, Moser E (1997) J Magn Res Imaging 7:1094
51. McLachlan GJ (1992) Discriminant Analysis and Statistical Pattern Recognition, Wiley, New York
52. Shaw RA, Mansfield JR, Jupriyanov VV, Mantsch HH (2000) Bioinorg Chem (in press)
53. Kupriyanov VV, Shaw RA, Xiang B, Mantsch HH, Deslauriers R (1997) J Mol Cell Cardiol 29:2431
54. Mendelsohn R, Paschalis EP, Boskey AL (1999) J Biomed Optics 4:14